Pergamon

Int. J. Heat Mass Transfer. Vol. 37, No. 7, pp. 1063–1071, 1994

0017-9310/94 $6.00 + 0.00

0017-9310(93)E0044-H

Boundary element analysis of thermocapillary convection with a free surface in a rectangular cavity

WEN-QIANG LU

Department of Physics, Division of Thermal Science, Graduate School, Chinese Academy of Sciences, P.O. Box 3908, Beijing 100039, China

(*Received for publication* 30 *November* 1993)

Abstract—A boundary element method for analysing thermocapillary convection with a free surface has been developed. The divergence theorem is applied to the non-linear convective volume integral in the boundary element formulation with the pressure penalty function. Consequently, velocity and temperature gradients are eliminated and the complete formulation is written in terms of velocity and temperature. This provides considerable reduction in storage and computational requirements while improving accuracy. Employing this method, a simulation of surface tension driven convective flow in a rectangular cavity with differential heated isothermal lateral walls in a microgravity environment has been demonstrated. The influence of different Marangoni numbers, Reynolds numbers and Prandtl numbers on the shape of the free surface, the temperature distribution and the flow fields has also been studied.

INTRODUCTION

THERMAL convection is a basic problem in thermal science. There are two kinds of thermal convection in a rectangular cavity with differently heated lateral walls: buoyancy convective flow and thermocapillary convective flow. However, the thermocapillary convection becomes the dominant convection in microgravity and micro-scale environment. It is a surface tension driven convective flow. A gradient of surface tension is produced by the difference of temperatures along the free surface and drives the flow along this surface. The flow propagates to the inner region of the cavity, therefore causing convection in the cavity. The study of this convective flow has important practical significance, for example, in space processing of electric materials.

Recently, reviews and investigations on problems in this field have been made [1–3]. Experiments of thermocapillary convection in rectangular cavity have been performed in space [4, 5] and in laboratories [6, 7]. Numerical modelings of these problems have been done by the finite difference method (FDM) [8–13] and finite element method (FEM) [14, 15], respectively. However, they only calculated the convection with flat or slightly deformed free surface [8–11, 15], and some limitations of the parameters are assumed. For example, a very low P_r was chosen in ref. [10]; although a wide range of P_r was chosen in ref. [11], but very small capillary number and a flat at leading order free surface were considered. In ref. [14], the effect of deformed free surface on thermocapillary convection was considered, but Marangoni numbers were limited to lower than 400, moreover, when the effect of P_r on the free surface was further considered, zero $R_e - M_a$ was chosen. In ref. [13], high M_a numbers were considered, however, very low capillary number ($= 10^{-3}$) was chosen, so that a fixed free surface shape has to be assumed to maintain its static shape of constant curvature. In ref. [12], the effects of fixed convex- and concave-free surface shapes for a unit P_r fluid were considered; however, the convergence beyond a Marangoni number of 10^3 had not been reached.

It is well known that the computational accuracy is lost in the region of high Reynolds number since the scheme of convective discretization introduces numerical diffusion in FDM and FEM. In order to reduce the numerical diffusion, some new schemes for discretizing convective terms have been developed such as QUICK [16] and QUICKER [17]. There are many difficulties in solving the free surface problems at middle and high R_e and further study is necessary.

The boundary element method (BEM) has provided potential advantages of storage and computational requirements over FDM and FEM. Therefore, many scientists have endeavored to raise the computational advantages of BEM.

Viscous flow problems, including thermal convection, are typical non-linear problems. In order to solve these problems, Kitagawa *et al.* [18, 19] developed the boundary element formulation by the basic solution of the Navier equations in elasticity with the penalty function of pressure terms. The calculation of the convective terms is the most important point when solving these problems at high Reynolds numbers. In [18], finite difference schemes and a boundary element iterative scheme (BEIS) were applied to calculate convective terms and compare the advantages of using upwind or central difference schemes and BEIS. As shown in the numerical results, BEIS of the convective terms is the most accurate of the two approaches. However, the computation is complex.

The first objective of this study is to fill a gap in solving the thermocapillary convection of an open

NOMENCLATURE

B_i Biot number
C_a $(\mu^* U_0^*/\sigma_0^*) = H^*/L^*$
g^* the gravity acceleration
G_r Grashof number, $\rho^{*2} g^* \bar{\omega}^* \Delta\theta^* H^{*3}/\mu^{*2}$
H^* the initial y_f at x-center position
L^* the length of the cavity
M_a Marangoni number, $P_r R_e$
n_j unit normal components
p^* pressure
P_r Prandtl number, $\mu^*/\rho^*\kappa^*$
q $\theta_{,n}$
R_e Reynolds number, $U_0^*\rho^* H^*/\mu^*$
r the distance between ξ and η
t_i^* the traction, $\sigma_{ij}^* n_j$
T_{ij}, U_{ij} Kelvin's solution
U_0^* Marangoni velocity, $-H^*\Delta\theta^*\sigma_T'/L^*\mu^*$
v_i velocity
x, y Cartesian coordinates.

Greek symbols
$\alpha_{ij}(\xi)$ δ_{ij} for $\xi \in A$
$\alpha_{ij}(\xi)$ $\frac{1}{2}\delta_{ij}$ for $\xi \in \Gamma$
β the angle included between τ and x
δ_{ij} the Kronecker delta symbol
ζ the curvature of free surface
η computational grade points
θ^* temperature
$\Delta\theta^*$ temperature difference $\theta_l^* - \theta_r^*$
Θ $\ln r$
κ^* the thermal diffusivity
λ the penalty parameter
μ^* the absolute viscosity
ξ computational grade points
ρ^* density
σ_{ij}^* the stress tensor
σ_T' the temperature coefficient of σ_0^*
σ_0^* the surface tension
τ_i unit tangential components
$\chi(\xi)$ 2π for $\xi \in A$
$\chi(\xi)$ π for $\xi \in \Gamma$
$\bar{\omega}^*$ the coefficient of expansion.

Superscripts
* dimensional variables
blank non-dimensional variables
li liquid
g gas
m iterative steps
0 initial values.

Subscripts
f free surface
b bottom
r right
l left.

rectangular cavity: simulating the thermocapillary convection with a free surface in the region of widely varying physical parameters—Marangoni numbers, Reynolds numbers and Prandtl numbers. An immediate objective of this research is to model the thermocapillary convection in crystal-growth techniques. The analytical or numerical study of the free surface problem in crystal-growth techniques is very difficult. We shall restrict ourselves to the model problem of the open-boat type crystal growth technology, and we only study the gas–melt free boundary, assuming a flat crystal–melt interface shape. The free surface problem of open-boat type is simplified as the free surface problem in an open rectangular cavity. The left vertical boundary of the cavity can be interpreted as the crucible wall. The right vertical boundary of the cavity can be interpreted as the melt–crystal interface. The temperatures equal to θ_l and θ_r, respectively.

Another objective of this work is to develop a boundary element method to solve these problems at middle and high R_e, P_r. On the basis of the BEM with the pressure penalty function [18], we improved the method for computing the convective terms. The divergence theorem is applied to the non-linear convective volume integral, so that velocity and temperature gradients are eliminated. The complete formulation is written in terms of velocity and temperature. Consequently, this provides considerable reduction in storage and computational requirements while improving accuracy. We applied the normal stress balance condition as the iterative equation of the free surface such as in ref. [20] and have successfully calculated the isothermal free surface problems at middle R_e [21, 22] and thermocapillary convection in a two-layer immiscible fluid system [23]. In this paper, this method is extended to calculate more complex non-linear problems, such as problems with a temperature gradient on the free surface. On the free surface, the temperature dependence of the surface tension must be taken into account, non-homogeneous surface tension drives the convective flow. Since gradients of surface tension appear on the free surface, the stress balance conditions become more complex. The non-linear momentum equations and energy equation are coupled with the free surface problem. The non-linear character of the problem is thus enhanced.

In this paper we successfully calculated thermocapillary convection with a free surface in an open rectangular cavity with viscous liquid in microgravity environment. Some important numerical results are presented.

BASIC EQUATIONS

One considers a system consisting of a steady incompressible viscous liquid in a rectangular cavity with differentially heated isothermal lateral walls (the temperature difference is $\Delta\theta^*$). On the basis of the basic laws of fluid mechanics and Boussinesq's approximation, the governing equations of this problem can be described by a tensor notation and a non-dimensional form as follows:

Continuity equation

$$v_{j,j} = 0 \tag{1}$$

Momentum equations

$$v_j v_{i,j} + p_{,i} - \frac{1}{R_e}(v_{i,j} + v_{j,i})_{,j} - \delta_{iy}\frac{G_r\theta}{R_e^2} = 0 \tag{2}$$

Energy equation

$$v_j\theta_{,j} - \frac{1}{M_a}\theta_{,jj} = 0 \tag{3}$$

where the lengths and velocity are scaled with respect to H^* and U_0^*, respectively. The relation between pressure p^* and non-dimensional pressure p is $p = (p^* + \rho^* g^* y^*)/\rho^* U_0^{*2}$. $U_0^* = (-H^*\Delta\theta^*\sigma_T'/L^*\mu^*)$, where H^* is the initial height of the free surface at x-center position, L^* is the length of the cavity, σ_T' is the temperature coefficient of the surface tension of the liquid, μ^* is the absolute viscosity. The parameters are: Reynolds number $R_e = (\rho^* U_0^* H^*/\mu^*)$, Prandtl number $P_r = (\mu^*/\rho^*\kappa^*)$, Marangoni number $M_a = R_e P_r$, and Grashof number $G_r = (\rho^{*2} g^* \bar{\omega}^* \Delta\theta^* H^{*3}/\mu^{*2})$, where ρ^*, κ^*, g^* and $\bar{\omega}^*$ are liquid density, thermal diffusivity, gravity acceleration and coefficient of expansion, respectively. In equation (3), $\theta = (\theta^* - \theta_r^*)/\Delta\theta^*$, $\Delta\theta^* = \theta_l^* - \theta_r^*$, θ^* is the temperature, subscripts l and r refer to the left and right boundaries, respectively.

One uses a penalty function technique [18] to calculate the pressure.

$$p = -\lambda v_{i,i} \tag{4}$$

where λ is the penalty parameter. Taking a large value of λ will make $v_{i,i}$ approach zero and satisfy mass conservation in an approximate manner. Substituting equation (4) into (2), one obtains:

$$\left(\lambda + \frac{1}{R_e}\right)v_{j,ji} + \frac{1}{R_e}v_{i,jj} = v_j v_{i,j} - \delta_{iy}\frac{G_r\theta}{R_e^2}. \tag{5}$$

Equations (5) are similar to the Navier equations of elasticity.

BOUNDARY INTEGRAL EQUATIONS

Applying the well-known Kelvin's fundamental solution of the Navier equations and the weighted residual approach, equations (5) are transformed into the following integral equations:

$$\int_A \left[\left(\lambda + \frac{1}{R_e}\right)v_{j,ji} + \frac{1}{R_e}v_{i,jj} - v_j v_{i,j} + \delta_{iy}\frac{G_r\theta}{R_e^2}\right]U_{ki}\,dA = 0. \tag{6}$$

Employing the Gauss divergence theorem, one obtains the following integral equations:

$$\alpha_{ij}v_j(\xi) + \int_\Gamma T_{ij}(\xi,\eta)v_j(\eta)\,d\Gamma - \int_\Gamma U_{ij}(\xi,\eta)t_j(\eta)\,d\Gamma = \int_A U_{ij}(\xi,\eta)\left(v_k(\eta)v_{j,k}(\eta) - \delta_{iy}\frac{G_r\theta}{R_e^2}\right)dA. \tag{7}$$

The convective terms appear in the domain integral of equations (7). The values of these convective terms can be obtained either by writing integral equations directly for $[v_j v_{i,j}]$, or by employing finite difference scheme [18]. The former is more complex in calculation, but the latter loses the accuracy. One uses the divergence theorem to the domain integrals in (7).

$$\int_A U_{ij}v_k v_{j,k}\,dA = \int_\Gamma U_{ij}v_k v_j n_k\,d\Gamma - \int_A U_{ij,k}v_k v_j\,dA.$$

Then, equations (7) are transformed into:

$$\alpha_{ij}(\xi)v_j(\xi) + \int_\Gamma T_{ij}(\xi,\eta)v_j(\eta)\,d\Gamma(\eta) - \int_\Gamma U_{ij}(\xi,\eta)[v_k(\eta)v_j(\eta)n_k(\eta) + t_j(\eta)]\,d\Gamma(\eta) = -\int_A \left[U_{ij,k}(\xi,\eta)v_k(\eta)v_j(\eta) + U_{ij}(\xi,\eta)\delta_{iy}\frac{G_r\theta}{R_e^2}\right]dA(\eta) \tag{8}$$

where $\alpha_{ij}(\xi) = \delta_{ij}$ for $\xi \in A$, $\alpha_{ij}(\xi) = \frac{1}{2}\delta_{ij}$ for $\xi \in \Gamma$, and δ_{ij} is the Kronecker delta symbol. These fundamental solutions U_{ij}, T_{ij} are known as Kelvin's solutions and have the form:

$$U_{ij} = -\frac{1}{8\pi(1-\phi)\gamma}[(3-4\phi)\ln r\delta_{ij} + r_{,i}r_{,j}] \tag{9}$$

$$T_{ij} = -\frac{1}{4\pi(1-\phi)r}[((1-2\phi)\delta_{ij} + 2r_{,i}r_{,j})r_{,n} - (1-2\phi)(r_{,i}n_j - r_{,j}n_i)] \tag{10}$$

where $\phi = (\lambda/2(\lambda + (1/R_e)))$, $\gamma = 1/R_e$, $r = |\xi - \eta|$, and n_k is the direction cosines of the outward normal to the boundary of the domain. One can express the differentials of Kelvin's solution as:

$$U_{ij,k} = -\frac{1}{8\pi(1-\phi)\gamma r}[(3-4\phi)\delta_{ij}r_{,k} + 2r_{,i}r_{,k}r_{,j} - \delta_{ki}r_{,j} - \delta_{kj}r_{,i}]. \tag{11}$$

One notes that velocity gradients are eliminated. The complete formulation is written in terms of

velocity. Consequently, this provides considerable reduction in storage and computational requirements while improving accuracy.

Applying Green's second theorem, a similar boundary integral equation equivalent to Poisson equation can be found for energy equation (3).

$$\chi\theta - \int_\Gamma \Theta_{,n}\theta \, d\Gamma + \int_\Gamma \Theta\theta_{,n} \, d\Gamma = M_a \int_A \Theta v_k \theta_{,k} \, dA. \tag{12}$$

Similarly, using the divergence theorem to the domain integral with convective term, one obtains

$$\int_A \Theta v_k \theta_{,k} \, dA = \int_\Gamma \Theta v_k \theta n_k \, d\Gamma - \int_A \Theta_{,k} v_k \theta \, dA. \tag{13}$$

Then, equation (12) is transformed into:

$$\chi(\xi)\theta(\xi) - \int_\Gamma \Theta_{,n}\theta \, d\Gamma + \int_\Gamma \Theta(q - M_a \theta v_k n_k) \, d\Gamma = -M_a \int_A \theta \Theta_{,k} v_k \, dA \tag{14}$$

$$q = \theta_{,n}$$

where $\chi(\xi) = 2\pi$ for $\xi \in A$, and $\chi(\xi) = \pi$ for $\xi \in \Gamma$. The fundamental solution is known as the solution of Poisson equation:

$$\Theta = \ln r. \tag{15}$$

One notes that temperature gradients are also eliminated. Therefore, the same advantages appear.

DISCRETIZATION OF BOUNDARY INTEGRAL EQUATIONS

In order to solve boundary integral equations (8) and (14), one divides boundary (Γ) and domain (A) into smooth line segments (Γ_j) and corresponding triangular cells, respectively. Then, boundary integral equations (8) and (14) can be discretized as the following algebraic equations:

$$A_{ij}v_{yj} + B_{ij}v_{xj} + C_{ij}t_{yj} + D_{ij}t_{xj} = W_{yi} \tag{16}$$

$$E_{ij}v_{yj} + F_{ij}v_{xj} + G_{ij}t_{yj} + H_{ij}t_{xj} = W_{xi} \tag{17}$$

$$X_{ij}\theta_j + Z_{ij}q_j = W_{\theta i} \tag{18}$$

$$A_{ij} = \alpha_{yy} + \int_{\Gamma_j} T_{yy}(\xi_i, \eta_j) \, d\Gamma \tag{19}$$

$$B_{ij} = \int_{\Gamma_j} T_{yx}(\xi_i, \eta_j) \, d\Gamma \tag{20}$$

$$C_{ij} = -\int_{\Gamma_j} U_{yy}(\xi_i, \eta_j) \, d\Gamma \tag{21}$$

$$D_{ij} = -\int_{\Gamma_j} U_{yx}(\xi_i, \eta_j) \, d\Gamma \tag{22}$$

$$E_{ij} = \int_{\Gamma_j} T_{xy}(\xi_i, \eta_j) \, d\Gamma \tag{23}$$

$$F_{ij} = \alpha_{xx} + \int_{\Gamma_j} T_{xx}(\xi_i, \eta_j) \, d\Gamma \tag{24}$$

$$G_{ij} = -\int_{\Gamma_j} U_{xy}(\xi_i, \eta_j) \, d\Gamma \tag{25}$$

$$H_{ij} = -\int_{\Gamma_j} U_{xx}(\xi_i, \eta_j) \, d\Gamma \tag{26}$$

$$X_{ij} = \chi(\xi_i) - \int_{\Gamma_j} \Theta_{,n}(\xi_i, \eta_j) \, d\Gamma \tag{27}$$

$$Z_{ij} = \int_{\Gamma_j} \Theta(\xi_i, \eta_j) \, d\Gamma \tag{28}$$

$$W_{yi} = \sum_j \left[-v_k(\eta_j)v_l(\eta_j) \int_{A_j} \left[U_{yl,k}(\xi_i, \eta) + U_{yl}(\xi_i, \eta) \frac{G_r\theta}{R_e^2} \right] dA - v_y(\eta_j)v_k(\eta_j)n_k(\eta_j)C_{ij} - v_x(\eta_j)v_k(\eta_j)n_k(\eta_j)D_{ij} \right] \tag{29}$$

$$W_{xi} = \sum_j \left[-v_k(\eta_j)v_l(\eta_j) \int_{A_j} U_{xl,k}(\xi_i, \eta) \, dA - v_y(\eta_j)v_k(\eta_j)n_k(\eta_j)G_{ij} - v_x(\eta_j)v_k(\eta_j)n_k(\eta_j)H_{ij} \right] \tag{30}$$

$$W_{\theta i} = \sum_j \left[-M_a\theta v_k(\eta) \int_{A_j} \Theta_{,k}(\xi_i, \eta) \, dA + M_a\theta(\eta_j)v_k(\eta_j)\eta_k(\eta_j)Z_{ij} \right]. \tag{31}$$

Equations (16)–(18) represent $3N$ equations for $6N$ unknown v_{yj}, v_{xj}, t_{yj}, t_{xj}, θ_j, q_j. The remaining equations must come from the boundary conditions. Hence, three boundary conditions must be specified at every grid point. On the free surface, one shall adopt an iterative determination; therefore one must employ a fourth condition—the normal stress balance condition to update the free surface at each iteration except that three conditions must be imposed.

BOUNDARY CONDITIONS

On the free surface S_f

There is no momentum transfer across the free surface, so

$$v_y = v_x \operatorname{tg} \beta. \tag{32}$$

The heat radiation condition is:

$$-q = \frac{B_i}{\Delta\theta^*}(\theta^{*4} - \theta_e^{*4}) \tag{33}$$

where B_i is Biot number, $B_i = (\varepsilon \Xi \Delta\theta^{*3} H^*/k)$, ε, Ξ and k are the emissivity, Stefan–Boltzmann constant and the thermal conductivity, respectively. θ_e^* is ambient gas temperature.

The tangential stress balance condition is $\sigma_{ij}^{*li} n_j \tau_i - \sigma_{ij}^{*g} n_j \tau_i = \nabla \sigma_0^* \tau_i$, where n_j and τ_i are unit normal and tangential vectors, respectively. The stress tensor is $\sigma_{ij}^* = -p^* \delta_{ij} + 2\mu e_{ij}^*$, $e_{ij}^* = (v_{i,j}^* + v_{j,i}^*)/2$. The traction is $t_i^* = \sigma_{ij}^* n_j$. The tangential stress balance condition can be transformed into $t_i^{*li} \tau_i - t_i^{*g} \tau_i = \nabla \sigma_0^* \tau_i$. The surface tension σ_0^* is assumed to vary linearly with the temperature. Therefore one obtains the following balance condition of the tangential stress on the free surface: $(t_i^{*li} - t_i^{*g}) \tau_i = \sigma_T' (\partial\theta^*/\partial\tau)$. If the surface tension is scaled with respect to σ_{Ts}^*, $\sigma_{Ts}^* = \sigma_{Ts}' \Delta\theta^*$, where s = li, g refer to liquid and gas, respectively, then one obtains the following non-dimensional form of the tangential stress balance condition: $C_a[\sigma_T^* t_i \tau_i] = \sigma_T^* (\partial\theta/\partial\tau)$. If gas viscosity is further eliminated, then the tangential stress balance condition is simplified as

$$C_a t_i \tau_i = \frac{\partial\theta}{\partial\tau} \tag{34}$$

where

$$C_a = \frac{\mu^* U_0^*}{\sigma_T^*} = \frac{H^*}{L^*}, \quad [x] = x^{li} - x^g.$$

The normal stress balance condition is $\sigma_{ij}^{*li} n_j n_i - \sigma_{ij}^{*g} n_j n_i = \nabla \sigma_0^* n_i + \sigma_0^* \zeta^*$, where ζ^* is the curvature of the free surface. One obtains the following non-dimensional form of the normal stress balance condition:

$$\zeta = \frac{C_a}{\theta} t_i n_i - \frac{1}{\theta} \frac{\partial\theta}{\partial n}. \tag{35}$$

In order to calculate the shape of the free surface, one needs to employ the following relation between the curvature of the free surface and the angle β that the tangent τ of the free surface makes with the coordinate x (see Fig. 1).

$$\sin[\beta(x)] = \int_0^x \zeta(x)\, dx. \tag{36}$$

One has fixed the contact angle at 180°, and, on the basis of mass conservation, one obtains the relation: $\int_0^{A^*} y_f(x)\, dx = \overline{V}_a$, where $A^* = (L^*/H^*) = C_a^{-1}$, $\overline{V}_a$ is the volume of the liquid; so one obtains the iterative equation of the free surface:

$$y_f = y_0 + \int_0^x [\mathrm{tg}\,(\beta)]\, dx \tag{37}$$

$$y_0 = C_a \overline{V}_a - C_a \int_0^{A^*} dx \int_0^x [\mathrm{tg}\,(\beta)]\, dx.$$

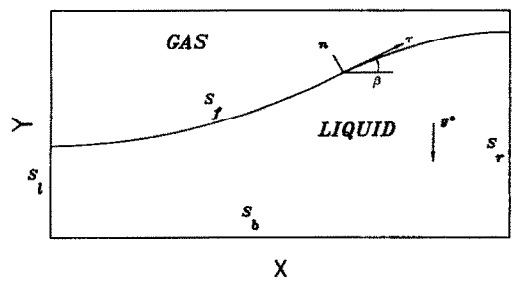

FIG. 1. Schematic for thermocapillary convection with a free surface in cavity.

On the bottom wall S_b

$$v_y = 0, \quad v_x = 0, \quad q = 0. \tag{38}$$

On the left wall S_l

$$v_y = 0, \quad v_x = 0, \quad \theta = 1. \tag{39}$$

On the right wall S_r

$$v_y = 0, \quad v_x = 0, \quad \theta = 0. \tag{40}$$

NUMERICAL ALGORITHM OF THE PROBLEM

One writes equations (16)–(18) in abbreviated form as

$$L\psi = \omega(\psi) \tag{41}$$

where ψ is the unknown.

There are several schemes of solving non-linear equation systems.

Newton–Raphson scheme:

$$\Pi(\psi^m)\psi^{m+1} = \Pi(\psi^m)\psi^m - L^*(\psi^m)$$
$$L^*(\psi) = L\psi - \omega(\psi)$$
$$\Pi(\psi) = \frac{\partial L^*(\psi)}{\partial\psi}. \tag{42}$$

The quasi-Newton scheme with Broyden's update [14, 24]:

$$\psi^{m+1} = J_m^{-1} \psi^m \tag{43}$$

$$J_m^{-1} = J_{m-1}^{-1} + \frac{(\vartheta_m - J_{m-1}^{-1} \varrho_m) \vartheta_m^T}{\vartheta_m J_{m-1}^{-1} \varrho_m} J_{m-1}^{-1}$$
$$\vartheta_m = \psi^m - \psi^{m-1}$$
$$\varrho_m = L^*(\psi^m) - L^*(\psi^{m-1})$$
$$J_0^{-1} \equiv \Pi^{-1}(\psi^0). \tag{44}$$

Since the problem has strong non-linear character, in order to achieve better convergence it is necessary to use non-linear iterative methods such as the Newton–Raphson scheme; however, it requires the calculation, assembly and inverse of the Jacobian matrix $\Pi(\psi)$ at each iterative step. The quasi-Newton method with Broyden's update can greatly reduce computational cost and the convergence rate approaches the same as the Newton–Raphson method. A detailed description of the method was presented in ref. [24], and the method was applied to calculate the non-linear equation systems of the finite element discretization in ref. [14].

One calculates the thermocapillary convection in an

open cavity by the iterative method that includes the following steps.

(1) Given the initial free surface and given the initial velocities and temperatures at nodal points, calculate the matrices including Green's function U_{ij}, T_{ij}, Θ_{ij}, $U_{ij,k}$ and $\Theta_{ij,k}$ by accurate Gaussian quadrature [25].

(2) Solving simultaneous equations (16)–(18) by the use of the quasi-Newton scheme with Broyden's update, calculate unknown v_i or t_i, θ or q.

(3) Calculate new shape of the free surface by the use of equation (37).

(4) Examine the convergence of the shape of the free surface, if the results are not converged, apply the updated shape of the free surface to calculate the matrices and to restart the second step.

NUMERICAL RESULTS

The thermocapillary convection with flat free surface

In order to examine the efficiency of this method, one firstly calculates the thermocapillary convection in low Prandtl number liquid by the use of the quasi-Newton method with Broyden's update. The physical parameters are the same as the experimental conditions of Camel *et al.* [6]: $P_r = 0.015$; $G_r = 0$; $C_a = 0.016$ for $R_e < 100$, $C_a = 0.08$ for $2000 > R_e \geqslant 100$, $C_a = 0.16$ for $R_e \geqslant 2000$.

A typical distribution of grids on the boundaries for $C_a = 0.08$ is tabulated in Table 1.

Since the significant boundary layers exist along the free surface, walls and especially near the stagnation point on the cold wall at high M_a, R_e, a non-uniform grid is needed for the grid refinement near these boundaries. The smallest grid size on the cold corner is four times smaller than the one corresponding to a uniform grid. The mesh spacing is gradually increased away from the boundaries.

The shapes of free surfaces are assumed to be flat, which is true for low Prandtl number liquid as proved by the experiment of Camel *et al.* [6].

The convergence character for $C_a = 0.08$, $R_e = 1000$ is tabulated in Table 2. The convergence rate is almost quadratic.

Numerical results of the surface velocity at x-center

Table 1. The distribution of grid points for $C_a = 0.08$

S_l	S_r	S_b	S_f
15	15	77	77

Table 2. The convergence character for $C_a = 0.08$, $R_e = 1000$

Steps	1	2	3	4
$\max \lvert v_i^m - v_i^{m-1} \rvert$	0.23	0.31 (−1)	0.54 (−2)	0.32 (−4)

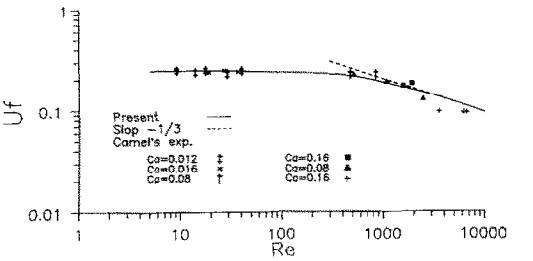

FIG. 2. Comparison of surface velocity at x-center to Camel's experimental data.

are presented in Fig. 2. As shown in Fig. 2, there is good agreement between our results and the experimental data of Camel *et al.* [6].

The velocity profiles at x-center position and the distributions of the surface velocities are drawn in Figs. 3 and 4, respectively. As shown in Figs. 3 and 4, in the low Reynolds numbers region, a full developed Poiseuille–Couette flow–Birikh's solution [6, 10] appears in central region. There are the accelerated and decelerated flow regions in the left and right lateral of central region, respectively. The length of the region of fully developed Poiseuille–Couette flow is reduced with increasing R_e; eventually the region of Birikh's solution disappears. These results are similar to ref. [10]. Agreement with experimental [6] and numerical [10] results would then justify our method as an important technique for this problem.

The thermocapillary convection with deformed free surface

A typical distribution of grids on the boundaries for $C_a = 1.0$ is tabulated in Table 3. The convergence

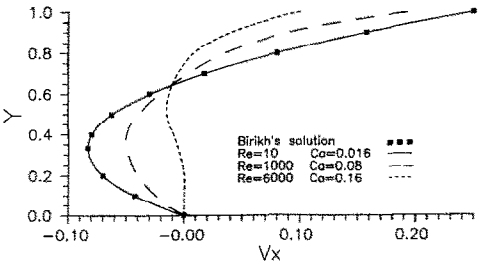

FIG. 3. Profiles of velocity V_x at x-center for various R_e at $P_r = 0.015$.

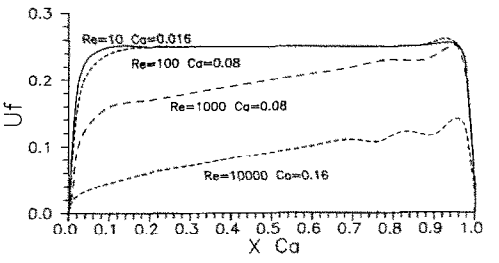

FIG. 4. Surface velocity distributions for various R_e at $P_r = 0.015$.

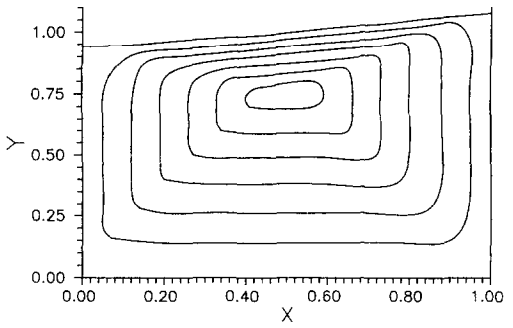

FIG. 5. Free surface and streamline map in thermocapillary convection for $M_a = 50$.

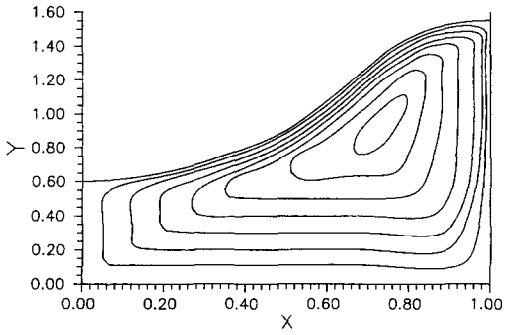

FIG. 6. Free surface and streamline map in thermocapillary convection for $M_a = 200$.

character for $P_r = 1.0$, $R_e = 1000$ is tabulated in Table 4.

The effects of the Marangoni–Reynolds numbers. One considers a pure Marangoni convection with the chosen physical parameters: $G_r = 0$, $P_r = 1.0$, $C_a = 1.0$, $B_i = 0$, $M_a = 50, 200, 1000, 2000$.

The influence of the Marangoni number on the free surface shape and flow fields is shown in Figs. 5 and 6.

As shown in Figs. 5 and 6, there are vorticity sources on the free surface; they propagate into inner flow fields, resulting in one clockwise vortex whose

Table 3. The distribution of grid points for $C_a = 1.0$

S_l	S_r	S_b	S_f
41	41	51	51

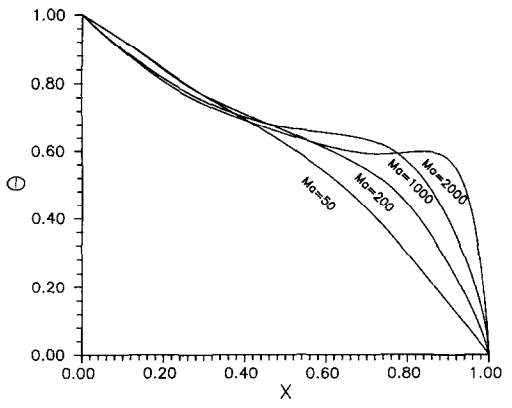

FIG. 7. Surface temperature distributions for various M_a at $P_r = 1.0$.

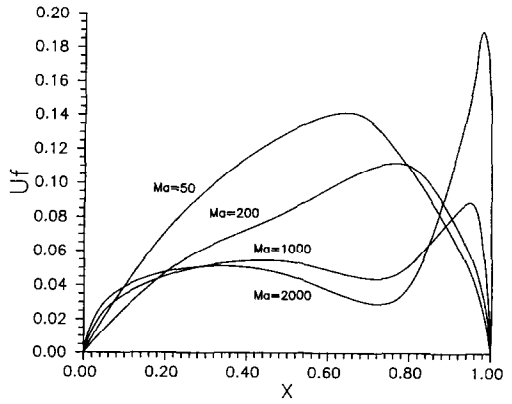

FIG. 8. Surface velocity distributions for various M_a at $P_r = 1.0$.

center is situated near the free surface. The vortex center moves towards the cold wall with increasing M_a.

The distributions of temperature and velocity on the free surface are drawn in Figs. 7 and 8, respectively. There are large temperature gradients in both corners since boundary layers exist, and notice that the temperature gradient at the cold corner is higher than at the hot corner. In this region the high temperature gradients produce local large driving forces leading to a local increase in surface velocity. Two maximums of surface velocity become obvious with increasing M_a.

The effects of the Prandtl numbers. The physical parameters are chosen as: $P_r = 0.05$, $R_e = 50$;

Table 4. The convergence character for $P_r = 1$, $R_e = 1000$

Outer iterations m	Inner iterations n	max $\lvert y_i^m - y_i^{m-1}\rvert$	$m = 2$ inner iteration	
1	5	0.15	n	max $\lvert v_i^n - v_i^{n-1}\rvert$
2	4	0.24 (−1)	1	0.90 (−1)
3	3	0.12 (−1)	2	0.21 (−1)
4	3	0.61 (−2)	3	0.43 (−2)
5	2	0.37 (−2)	4	0.19 (−4)
6	2	0.15 (−2)		
7	1	0.85 (−3)		

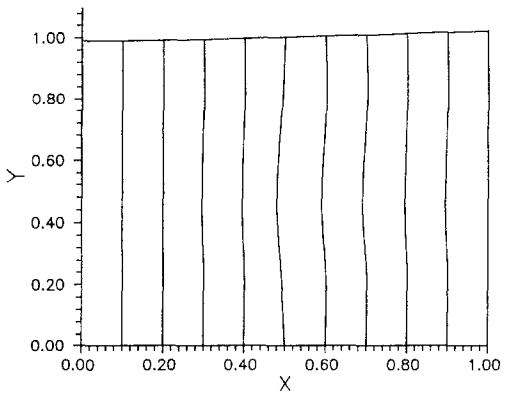

FIG. 9. The shape of the free surface and isotherm map for $P_r = 0.05$, $R_e = 50$.

$P_r = 50$, $M_a = 2500$; $C_a = 1$; $G_r = 0$; $B_i = 0$. As shown in Figs. 9 and 10, for $P_r = 0.05$, the shape of the free surface becomes flatter, and the isotherm approaches to a straight line, heat conduction is the main effect and heat convection can be eliminated; for $P_r = 50$, the isotherm is bent by the convection, and the free surface deflection is also different from buoyancy convection case as in Fig. 6 of ref. [14]. Notice that there are large temperature gradients on both corner of the free surface, especially on the right cold corner in Fig. 10, but such a picture does not appear in Fig. 9. These results show that the strong influences of Prandtl numbers on the free surface temperature distributions produce different thermocapillary flows, free surface shapes, flow structures and heat transport characters.

CONCLUSIONS

Employing the divergence theorem to the non-linear convective volume integral of the boundary element formulation, the velocity and temperature gradients are eliminated, and the complete formulation is written in terms of velocity and temperature. This provides considerable reduction in storage and computational requirements while improving accuracy. The non-linear equation systems of the boundary element discretization are solved by the quasi-Newton scheme with Broyden's update. Good agreement between our results and experimental [6] and numerical [10] results in the case of flat free surface at $P_r = 0.015$ is obtained. The method is further used to analyze the thermocapillary convection with a free surface. Some important numerical results are given. Especially, the effects of widely varying physical parameters: Marangoni numbers, Reynolds numbers and Prandtl numbers on the free surface shapes, velocity and temperature fields are presented.

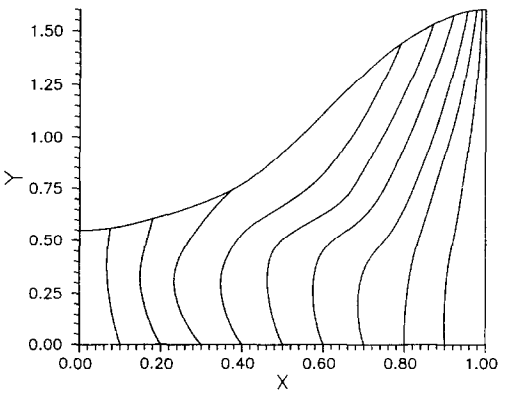

FIG. 10. The shape of the free surface and isotherm map for $P_r = 50$, $M_a = 2500$.

Acknowledgement—The project is supported by the National Natural Science Foundation of China.

REFERENCES

1. S. Ostrach, Low-gravity fluid flows, *Ann. Rev. Fluid Mech.* **14,** 313–345 (1982).
2. S. H. Davis, Thermocapillary instabilities, *Ann. Rev. Fluid Mech.* **19,** 403–435 (1987).
3. L. G. Napolitano, Surface and buoyancy driven free convection, *Acta Astronautica* **9**(4), 199–215 (1982).
4. M. C. Limbourg and P. H. Georis, Preliminary results of Texus 19(TEM06-8) experiment: Marangoni convection around a surface tension minimum, *Proceedings VIIth European Symposium on Materials and Fluid Sciences in Microgravity*, pp. 347–351, Oxford, U.K. (1989).
5. J. Metzger and D. Schwabe, Coupled buoyant and thermocapillary convection, *PhysicoChem. Hydrodyn.* **10,** 263–282 (1988).
6. D. Camel, P. Tison and J. J. Favier, Marangoni flow regimes in liquid metals, *Acta Astronautica* **13,** 723–726 (1986).
7. A. G. Kirdyashkin, Thermogravitational and thermocapillary flow in a horizontal temperature gradient, *Int. J. Heat Mass Transfer* **27,** 1205–1218 (1984).
8. J. L. Bergman and J. R. Keller, Combined buoyancy, surface tension flow in liquid metals, *Num. Heat Trans.* **13,** 49–63 (1988).
9. M. Strani, R. Piva and G. Graziani, Thermocapillary convection in a rectangular cavity: asymptotic theory and numerical simulation, *J. Fluid Mech.* **130,** 347–376 (1983).
10. H. Ben Hadid and B. Roux, Thermocapillary convection in long horizontal layers of low-Prandtl-number melts subject to a horizontal temperature gradient, *J. Fluid Mech.* **221,** 77–103 (1990).
11. B. M. Carpenter and G. M. Homsy, High Marangoni number convection in a square cavity: part 2, *Phys. Fluids A* **2,** 137–149 (1990).
12. J. R. Keller and J. L. Bergman, Thermocapillary cavity convection in wetting and nonwetting liquids, *Numerical Heat Transfer* **18**(A), 33–49 (1990).
13. Y. Kamototani and J. Platt, Effect of free surface shape on combined thermocapillary and natural convection, *J. Thermophys. Heat Transfer* **6**(4), 721–726 (1992).
14. C. Cuvelier and J. M. Driessen, Thermocapillary free boundaries in crystal growth, *J. Fluid Mech.* **169,** 1–26 (1986).
15. E. Crespo der Arco, G. P. Extremet and R. L. Sani, Thermocapillary convection in a two-layer fluid system with flat interface, *Adv. Space Res.* **11**(7), 129–132 (1991).
16. B. P. Leonard, A stable and accurate convective modeling procedure based on quadratic upstream interpolation, *Comp. Math. Appl. Mech. Engng* **12,** 59–78 (1979).

17. S. V. Pollard and A. L. W. Siu, The calculation of some laminar flows using various discretization schemes, *Comp. Math. Appl. Mech. Engng* **35,** 293–308 (1982).
18. K. Kitagawa, C. A. Brebbia, L. C. Wrobel and M. Tanaka, Boundary element analysis of viscous flow by penalty function formulation, *Engng Anal.* **3**(4), 194–200 (1986).
19. K. Kitagawa, C. A. Brebbia, L. C. Wrobel and M. Tanaka, Viscous flow analysis including thermal convection. In *Boundary Elements IX* (Edited by C. A. Brebbia, M. Tanaka and T. Honma), Vol. 2, pp. 459–476. Springer, Berlin (1987).
20. W.-Q. Lu and H.-C. Chang, An extension of the biharmonic boundary integral method to free surface flow in channels, *J. Comp. Phys.* 77(2), 340–360 (1988).
21. W.-Q. Lu, Simulation of solitary wave flow fields on free falling thin liquid film using boundary element method. In *Advances in Heat Pipe Science and Technology* (Edited by Ma, Tongze), pp. 54–59. International Academic Publishers, Beijing (1992).
22. W.-Q. Lu, Boundary element method of analysing nonlinear phenomena on gas–liquid two-phase free surface at middle and higher Reynolds numbers. In *Computational Modelling of Free and Moving Boundary Problems II* (Edited by L. C. Wrobel and C. A. Brebbia), pp. 167–176. Computational Mechanics Publications, Southampton, U.K. (1993).
23. W.-Q. Lu, Simulation of thermocapillary convection in a two-layer immiscible fluid system using a boundary element method, *J. Thermal Sci.* **1**(4), 259–266 (1992).
24. J. E. Dennis and J. More, Quasi-Newton methods, motivation and theory, *SIAM Rev.* **19,** 46–89 (1977).
25. C. A. Brebbia, J. C. F. Telles and L. C. Wrobel, *Boundary Element Techniques*. Springer-Verlag, Berlin (1984).